Molecular dynamics simulations informed by membrane lipidomics reveal the structure–interaction relationship of polymyxins with the lipid A-based outer membrane of *Acinetobacter baumannii*

Xukai Jiang[1], Kai Yang[2], Bing Yuan[2], Meiling Han [1], Yan Zhu [1], Kade D. Roberts[1], Nitin A. Patil[1], Jingliang Li[3], Bin Gong[4], Robert E. W. Hancock[5], Tony Velkov[6], Falk Schreiber[7], Lushan Wang[8] and Jian Li[1]*

[1]Biomedicine Discovery Institute, Infection & Immunity Program and Department of Microbiology, Monash University, Melbourne, Australia; [2]Centre for Soft Condensed Matter Physics and Interdisciplinary Research & School of Physical Science and Technology, Soochow University, Suzhou, China; [3]Institute for Frontier Materials, Deakin University, Geelong, Victoria, Australia; [4]School of Computer Science and Technology, Shandong University, Jinan, China; [5]Department of Microbiology and Immunology, University of British Columbia, Vancouver, Canada; [6]Department of Pharmacology & Therapeutics, University of Melbourne, Melbourne, Australia; [7]Department of Computer and Information Science, University of Konstanz, Konstanz, Germany; [8]State Key Laboratory of Microbial Technology, Shandong University, Qingdao, China

*Corresponding author. E-mail: Jian.Li@monash.edu

Background: MDR bacteria represent an urgent threat to human health globally. Polymyxins are a last-line therapy against life-threatening Gram-negative 'superbugs', including *Acinetobacter baumannii*. Polymyxins exert antimicrobial activity primarily via permeabilizing the bacterial outer membrane (OM); however, the mechanism of interaction between polymyxins and the OM remains unclear at the atomic level.

Methods: We constructed a lipid A-based OM model of *A. baumannii* using quantitative membrane lipidomics data and employed all-atom molecular dynamics simulations with umbrella sampling techniques to elucidate the structure–interaction relationship and thermodynamics governing the penetration of polymyxins [B_1 and E_1 (i.e. colistin A) representing the two clinically used polymyxins] into the OM.

Results: Polymyxin B_1 and colistin A bound to the *A. baumannii* OM by the initial electrostatic interactions between the Dab residues of polymyxins and the phosphates of lipid A, competitively displacing the cations from the headgroup region of the OM. Both polymyxin B_1 and colistin A formed a unique folded conformation upon approaching the hydrophobic centre of the OM, consistent with previous experimental observations. Polymyxin penetration induced reorientation of the headgroups of the OM lipids near the penetration site and caused local membrane disorganization, thereby significantly increasing membrane permeability and promoting the subsequent penetration of polymyxin molecules into the OM and periplasmic space.

Conclusions: The thermodynamics governing the penetration of polymyxins through the outer leaflet of the *A. baumannii* OM were examined and novel structure–interaction relationship information was obtained at the atomic and membrane level. Our findings will facilitate the discovery of novel polymyxins against MDR Gram-negative pathogens.

Introduction

The world is facing a serious health challenge due to antimicrobial resistance. The WHO and government sectors have developed a global action plan to mitigate antimicrobial resistance.[1] MDR *Acinetobacter baumannii* is a particularly problematic pathogen due to its resistance to almost all available antibiotics and sits atop the WHO priority pathogen list for research and development of new antibiotics.[2] Due to the lack of new antibiotics under development, polymyxins (i.e. polymyxin B and colistin; Figure 1a) are

increasingly used as a last-line option against life-threatening Gram-negative pathogens, including *A. baumannii*.[3] Although the interaction of polymyxins with bacterial membranes has been investigated over the last few decades,[4–7] the exact mechanism by which polymyxins penetrate into the bacterial outer membrane (OM) remains unclear at the atomic scale.

It is proposed that polymyxins cross the bacterial OM via 'self-promoted uptake', during which the displacement of divalent cations and membrane permeabilization play important roles.[8–10]
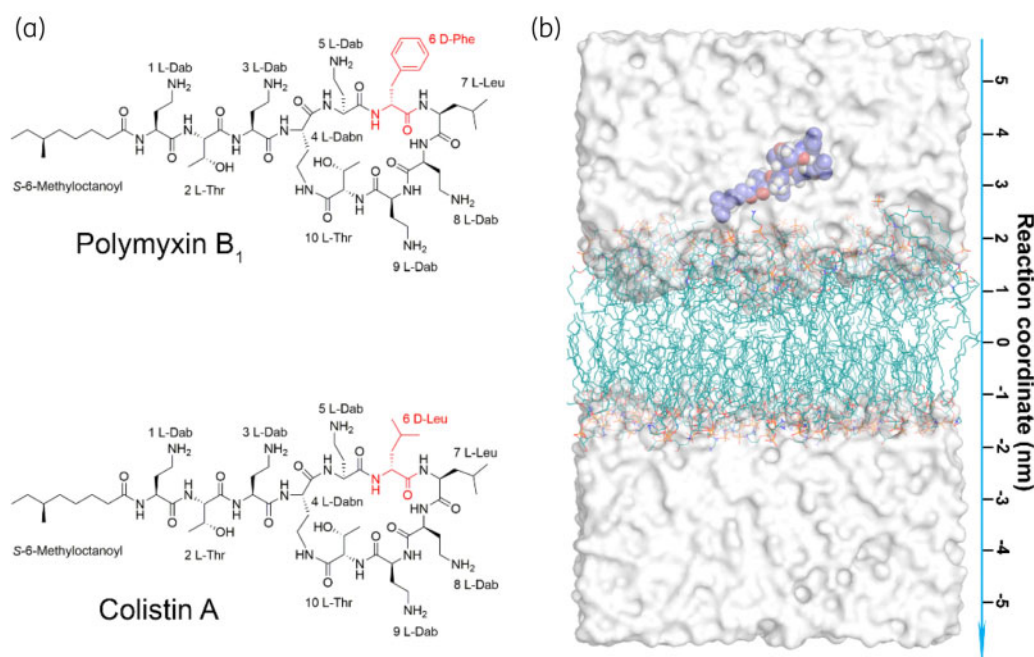
Figure 1. MD simulations system. (a) Chemical structures of polymyxin B$_1$ and colistin A. Polymyxins consist of an N-terminal fatty acyl tail, a linear tripeptide and a cyclic heptapeptide. The different residues at position 6 are depicted in red. (b) The simulation system includes a lipid bilayer, a single polymyxin molecule, water molecules and ions. The reaction coordinate is the distance between the centre of mass of the polymyxin molecule and the OM. The polymyxin molecule and OM lipids (including lipid A and phospholipids) are shown as blue spheres and teal lines, respectively. Water molecules are depicted by the white surface and ions are not shown for clarity. This figure appears in colour in the online version of *JAC* and in black and white in the print version of *JAC*.

There are several models for the interaction of antimicrobial cationic peptides with the bacterial cytoplasmic membrane, including the barrel-stave, toroidal pore, carpet and aggregate models;[11,12] however, none explains how the polymyxins penetrate the bacterial OM. Lipid A-based structure–activity relationship models were developed for polymyxins based on NMR data.[13,14] However, a major limitation of these models is that each polymyxin molecule only interacts with a single lipid A molecule, whereas biochemical assays indicate that the interaction is substantially more complicated.[15] This prevents a comprehensive illustration of the mode of action of polymyxins at the OM level.[14,16] Although the interactions of polymyxins with bacterial membranes have been investigated by various approaches, including fluorescent titration, neutron reflectometry and X-ray scattering,[17–19] they have failed to offer a dynamic view of the permeabilization of the bacterial OM by polymyxins. Molecular dynamics (MD) simulations, coupled with umbrella sampling techniques, provide a powerful approach to examine the exact mode of action of antimicrobial peptides with superior temporal and spatial resolution.[12,20,21] Limited by the conformational sampling ability of conventional MD simulations, previous simulation studies on polymyxins mainly characterized their interactions with the headgroups of membrane lipids without tracking their penetration into the hydrophobic region of the membrane.[5,6] Importantly, these previous studies often simplified the lipid composition of the membrane and neglected the importance of membrane heterogeneity for the interaction with polymyxins. Here, we developed an *A. baumannii* OM model using quantitative membrane lipidomics data[22] and employed all-atom MD simulations and umbrella sampling to elucidate how polymyxins interact

with the OM of *A. baumannii* and the thermodynamics governing the penetration into the OM.

Methods

System preparation

The heterogeneity of biological membranes plays an essential role in their interactions with antimicrobial peptides.[20,23] To build a realistic bacterial OM, quantitative membrane lipidomics data of *A. baumannii* were employed to set the lipid composition and chemotypes of its OM.[22] The methods of lipidomics analysis are available as Supplementary data at *JAC* Online. The molar ratio of various lipids in the outer leaflet of the OM contained 75% *hepta*-acyl lipid A (12:0, 12:0, 12:0, 14:0/12:0, 12:0, 14:0), 18% phosphatidylethanolamine (PE; 16:0/18:1), 4% phosphatidylglycerol (PG; 16:0/18:1) and 3% cardiolipin (CL; 16:0, 18:1/16:0, 18:1); the inner leaflet was composed of 72% PE, 16% PG and 12% CL. This lipidomics-informed membrane composition mimicked the OM of *A. baumannii*. Lipid A represents the conserved component of LPS and the major interaction target of polymyxins.[13] As our study aimed to examine the mechanism of interaction between polymyxins and the OM of susceptible isolates at the atomic level, WT lipid A was employed in our MD simulations. The topology parameters of these lipids are from CHARMM-GUI based on the all-atom CHARMM36 force field and the asymmetric membrane model was constructed using CHARMM-GUI *Membrane Builder* in a tetragonal box.[24] TIP3P water molecules and counter-ions were added to hydrate and neutralize the simulation system, respectively.

The structure of polymyxins was built using Chem3D and energy minimization was performed to relieve potential intramolecular steric clashes. We simulated polymyxin B$_1$ molecules in solution and found that their conformations were consistent with the reported conformational ensembles

(Figure S1, available as Supplementary data at *JAC* Online).[6] The topology parameters of polymyxins were generated using the SwissParam server.[25] The polymyxin molecule was placed above the bilayer using the internal Gromacs tool *gmx insert-molecules* by replacing water molecules.[26] The dimensions of the simulation box were approximately 7.6×7.6×12.7 nm. The details of the MD simulation systems are listed in Table S1.

Steered MD simulations

Steered MD simulations were employed in the present study to accelerate the penetration of polymyxins into the bacterial OM. This method has been widely used in examining antimicrobial peptide–membrane interactions.[12,20,27,28] In our simulations, a harmonic potential with a force constant of 500 kJ/mol/nm^2 was applied between the centre of mass of the polymyxin molecule and the membrane along the Z-axis,[29] which allowed the polymyxin molecule to penetrate the bacterial OM smoothly and achieve the unique conformational transition consistent with previous experimental observations.[14,16] For each OM–polymyxin interaction system, three independent simulation replicates were performed to examine the reproducibility of the simulation results. Figure 1(b) shows the initial configuration of the steered MD simulation system.

Umbrella sampling

Umbrella sampling simulations were conducted to calculate the free energy profile during penetration into the bacterial OM.[30,31] Snapshots from the steered MD simulations were generated and employed to initiate a series of simulation windows in which the centre of mass of the polymyxin molecule was harmonically restrained at a series of fixed Z values. The configuration used for each window was selected every 0.2 nm in the range $Z = 3.21/2.85$ nm (above the outer leaflet) to $Z = 0.01/−0.15$ nm (the hydrophobic centre), resulting in 17 and 16 simulation windows in the polymyxin B$_1$ and colistin A systems, respectively. Table S2 shows the details of simulation windows and the free energy profiles were calculated according to the WHAM integration algorithm.[32]

Simulation parameters

GROMACS 5.1.2 was used to perform all MD simulations with the CHARMM36 all-atom force field with the default deprotonated lipid A in CHARMM-GUI.[26,33] A recent study revealed that the protonation state of lipid A was a key factor in regulating the OM properties;[34] our preliminary simulation results showed that the protonation state of lipid A did not significantly affect the free energy profiles of the penetration of colistin A through the outer leaflet of lipid A-based OM (Figure S2). Energy minimization was performed using the steepest descent algorithm. A six-step equilibration process was carried out by gradually turning off the position restraints on lipid molecules. Periodic boundary conditions were considered and all simulations were conducted at constant temperature (313 K) and pressure (1 bar) using the Nosé–Hoover and semi-isotropic pressure coupling approach with Parrinello–Rhaman barostat.[35–37] The time constant of coupling for temperature and pressure was 1 and 5 ps, respectively. The Particle Mesh Ewald ('PME') method was employed to treat long-range electrostatic interactions with a short-range cut-off of 1.2 nm,[38] while the shifted Lennard–Jones potential algorithm was used to calculate the Van der Waals interactions with a general cut-off of 1.2 nm and a shifting cut-off of 1.0 nm. The trajectory in production simulations was recorded every 10 ps.

Results

Penetration of polymyxins into the OM of *A. baumannii*

Through a steered MD simulation technique, the penetration trajectories of polymyxin B$_1$ (Figure 2a) and colistin A (Figure 2b)

molecules into the bacterial OM were tracked. Following the initial placement of polymyxin molecules above the OM surface, they subsequently attached to the headgroup region of the OM and orientated their hydrophobic segments (i.e. fatty acyl tail, D-Phe6/Leu6 and L-Leu7) to face toward the OM centre. Successively, polymyxin B$_1$ and colistin A translocated to the hydrophobic centre of the OM and formed a folded conformation. During this process, the hydrophobic segments of each polymyxin molecule adopted an inward orientation and were surrounded by the hydrocarbon tails of the lipid A and phospholipids; meanwhile, the polar residues of polymyxins retained the interactions with the headgroups of lipid A and phospholipids in the outer leaflet of the OM. Notably, this folded conformation of polymyxins was also found in previous NMR studies of polymyxin–LPS interaction, although the observed conformation of the polymyxin molecule in the presence of only lipid A was slightly more compacted than observed in membranes with simulations.[14,16]

The interaction energy results clearly show that the electrostatic interaction between the positively charged Dab residues of the polymyxin molecule and the negatively charged phosphate groups on the OM was the key player for their initial interaction. Although the relative energy contribution of each residue varied slightly in different simulation replicates, L-Dab1, L-Dab5 and L-Dab8 were the major contributors to the interactions observed with polymyxin B$_1$ (Figure 2c and Figure S3) and L-Dab1, L-Dab3 and L-Dab9 were the major contributors to the interactions observed with colistin A (Figure 2d and Figure S3). Due to the repulsive effect between the water and hydrophobic residues, when polymyxins attached to the OM surface, the D-Phe6 in polymyxin B$_1$ was closer to the hydrophobic region of the lipid A molecules compared with D-Leu6 in colistin A. This slight difference in orientation may increase the possibility of L-Dab5 (sits adjacent to D-Phe6) in polymyxin B$_1$ interacting with the headgroups of lipid A molecules in the OM. As a result, L-Dab5 formed the strongest interaction with the OM among the polymyxin B$_1$ residues. Interestingly, the Ca^{2+} density was lowered in the binding area of polymyxin molecules on the x–y plane of the OM, indicating that both polymyxin B$_1$ and colistin A competitively displaced the Ca^{2+} from the OM when their Dab side chains bound to the OM headgroup region (Figure 2e). As divalent cations generally stabilize the bacterial OM as a major cross-linking agent between the neighbouring LPS molecules,[39,40] the displacement of Ca^{2+} by polymyxin B$_1$ and colistin A rendered the OM less stable and possibly enhanced the OM permeabilization.

Free energy profiles during the OM penetration of polymyxins

The overall trends of the free energy profiles were similar between polymyxin B$_1$ and colistin A (Figure 3a). During the initial movement of the polymyxin molecule from the water environment into the headgroup region of the OM, there was a slight decrease in free energy ($\Delta G_{PMB} = −4.08$ kcal/mol; $\Delta G_{colistin} = −3.01$ kcal/mol), reflective of the favourable electrostatic interactions between the cationic Dab residues on the polymyxin molecule and the negatively charged phosphate groups on lipid A in the OM. Subsequently, the free energy gradually increased as the polymyxin molecule passed through the headgroup region of the OM
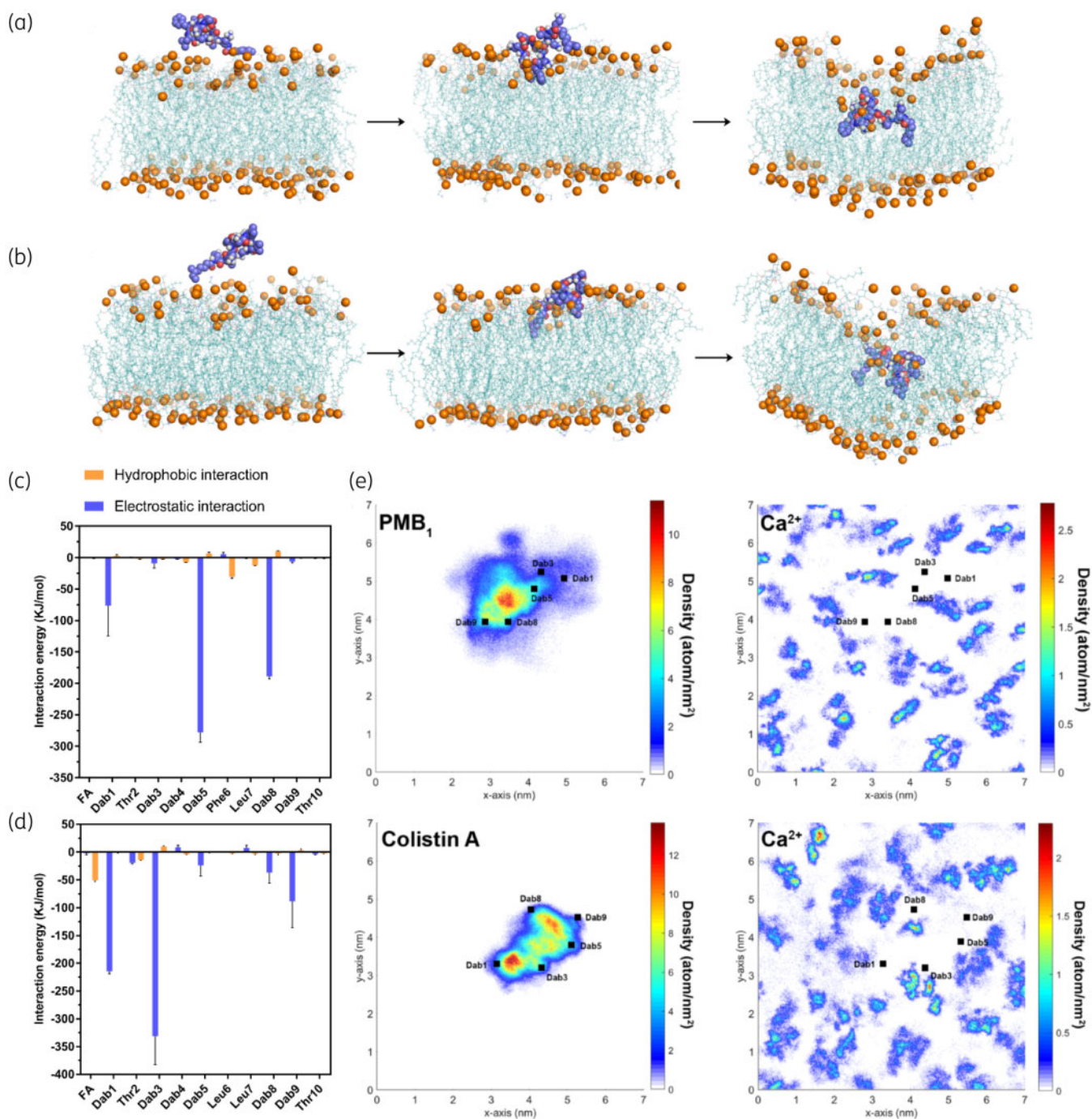
Figure 2. Polymyxin penetration into the bacterial OM. Representative snapshots showing the penetration of (a) polymyxin B_1 and (b) colistin A into the Gram-negative bacterial OM. Polymyxin molecules are shown as blue spheres with red oxygen atoms and white hydrogen atoms. The OM is shown as teal lines. The phosphate atoms are shown as orange spheres to indicate the position of the polymyxin molecule relative to the OM surface. Interaction energy between each residue of (c) polymyxin B_1 and (d) colistin A and the OM. (e) Density map of polymyxin molecules and Ca^{2+} on the $x–y$ plane of the OM. FA, fatty acyl. This figure appears in colour in the online version of *JAC* and in black and white in the print version of *JAC*.

outer leaflet. After this, the free energy substantially increased as the polymyxin molecule traversed the hydrophobic layer of the OM. Notably, there was a major difference in free energy profiles between polymyxin B_1 and colistin A. In the range from 0.91 to 1.67 nm, equivalent to the headgroup region of the OM outer leaflet, the free energy was approximately 55% higher with polymyxin B_1 than colistin A (e.g. 23.2 versus 15.0 kcal/mol at $Z = 1$ nm), indicating that colistin A traversed the polar headgroup region more readily than polymyxin B_1. This difference is very likely due to the different hydrophobicity and steric hindrance at position
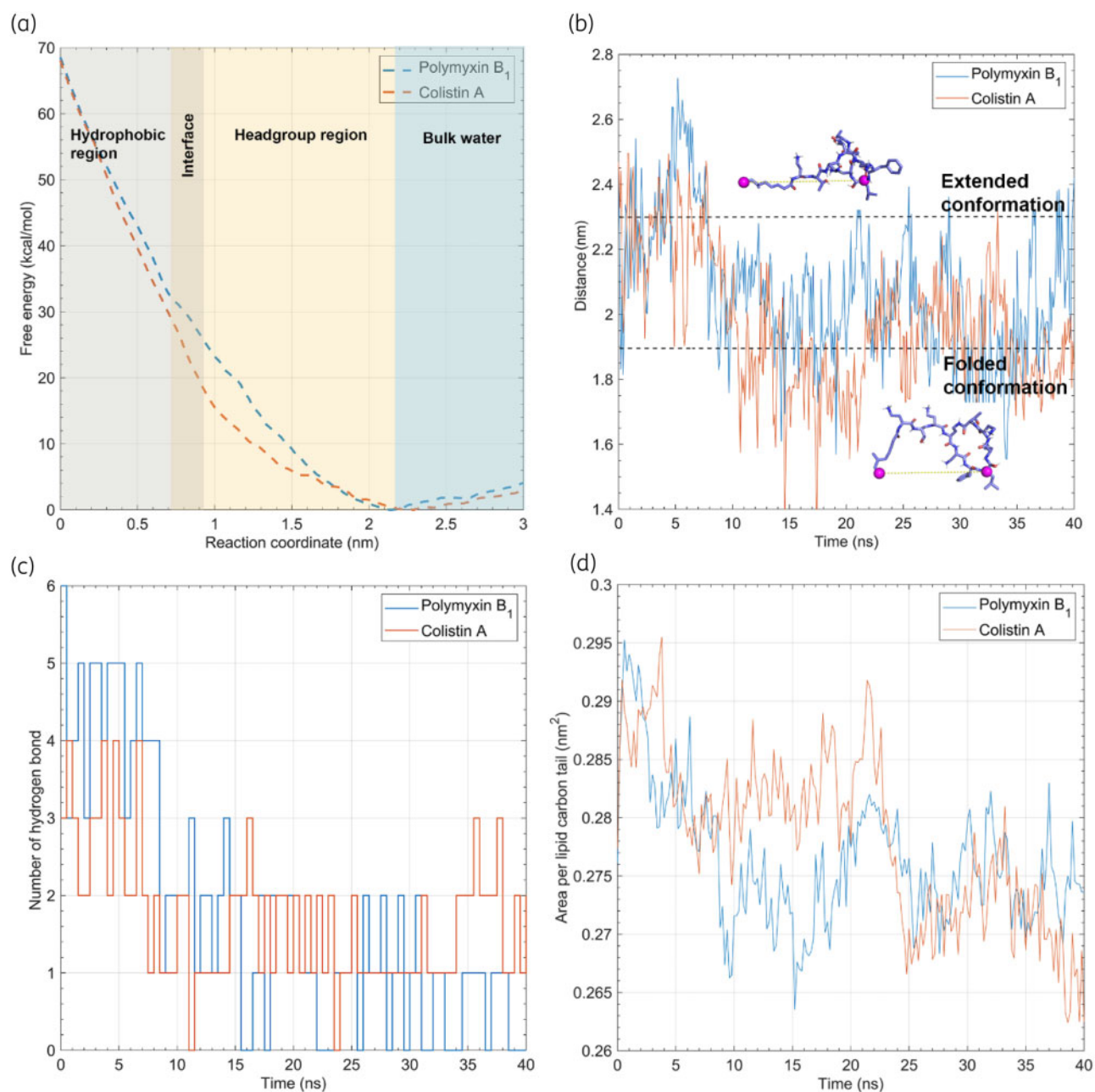
Figure 3. Thermodynamics governing the penetration of polymyxins. (a) Free energy profiles of polymyxin penetration into the OM. The free energy minimum is shifted to zero in the profiles. (b) Geometric distance between the atom pairs of polymyxins. The atoms used for the distance calculation are shown as purple spheres in the polymyxin B_1 structure. (c) Number of hydrogen bonds between the lipids that interact with the polymyxins and the rest of the OM. (d) Area per lipid carbon tail is calculated to indicate the packing density in the hydrophobic region of the OM. This figure appears in colour in the online version of *JAC* and in black and white in the print version of *JAC*.

6 (L-Phe6 in polymyxin B_1 versus L-Leu6 in colistin A; Figure 1a), which is the only structural difference between the two polymyxins.

As mentioned above, both polymyxin B_1 and colistin A adopted a folded conformation inside the OM. To characterize their conformational dynamics, the distance between the last carbon atom of the fatty acyl tail and the C_α of L-Leu7 of the polymyxin molecule was calculated (Figure 3b). When polymyxins entered the hydrophobic region of the OM, they experienced a significant conformational transition from an extended to a folded conformation with the latter being maintained during the subsequent penetration process, most likely due to the highly hydrophobic environment of the OM centre. This folded conformation was reproducible in different simulation replicates for polymyxin B_1 and colistin A (Figure S4)

and allowed the amphipathic polymyxin molecule to specifically interact with the negatively charged headgroups of lipid A and hydrophobic core of the OM.[41]

We further examined the number of intermolecular hydrogen bonds between the lipids interacting with the polymyxin molecule and the other lipids in the OM. Not surprisingly, the number of hydrogen bonds decreased from 3–5 to 0–2 upon the penetration of polymyxin B_1 and from 2–4 to 1–2 upon OM penetration of colistin A (Figure 3c), indicating a reduction in the intermolecular interactions between the lipid headgroups near the polymyxin penetration site on the OM. Meanwhile, the area per lipid carbon tail also decreased as the polymyxins penetrated into the OM (Figure 3d), reflective of the conformational constraint of the lipid A and phospholipid tails. These results indicate that the penetration of polymyxins primarily disorganized the headgroup region of the OM, while they increased the packing of the OM hydrophobic region, which is consistent with an earlier report.[42]

Atomic structure–interaction relationship of polymyxins with the OM of A. baumannii

Unlike previous NMR studies on LPS–polymyxin interaction,[14,16] in our MD systems the polymyxin molecule interacted with several different lipid A and phospholipid molecules in the OM (Figure 4). For polymyxin B_1, the five cationic Dab side chains formed polar contacts with the phosphate groups of three lipid A molecules and one cardiolipin molecule, whereas the hydrophobic triad (i.e. fatty acyl tail, D-Phe6 and L-Leu7) formed hydrophobic contacts with the hydrocarbon tails of the surrounding lipid A and phospholipid molecules (Figure 4a). Similarly, the five cationic Dab side chains of colistin A were close to the phosphate groups of four lipid A molecules and one cardiolipin molecule, with the hydrophobic triad embedded in the fatty acyl tails of lipid A and phospholipid molecules. The structure–interaction models generated from independent simulation replicates revealed that one polymyxin molecule primarily interacted with 3–4 lipid A molecules in the OM (Figure S4). Notably, in our OM-based interaction model the side chains of L-Dab3 and L-Dab5 of polymyxin B_1 and colistin A orientated towards the middle of the polymyxin molecule and were partly shielded by the hydrophobic triad, while L-Dab1, L-Dab8 and L-Dab9 were located at the edge of the polymyxin molecule and interacted with the phosphate groups of adjacent lipid A molecules, inducing reorientation of the headgroups of these lipid A molecules. Thus, the folded conformation of polymyxins allows effective interactions with both polar headgroups and hydrophobic carbon tails of multiple lipid A molecules and is thus a major intermediate step in the disorganization of the bacterial OM.

Polymyxins enhance the permeability of the OM of A. baumannii

The integral OM structure constituted a permeability barrier, preventing water molecules from entering into its hydrophobic region (Figure 5a). Along with the penetration of the polymyxin molecule, a local membrane deformation gradually formed, due to the strong electrostatic interactions between the polymyxin Dab side chains and the lipid A phosphate groups (Figure 5b and c and Figure S5). Consequently, water molecules and calcium ions

entered the hydrophobic region of the OM readily via the formed pore, significantly increasing the membrane permeability.

To test whether induced membrane pores promote the penetration of antimicrobial peptides,[43] we employed the polymyxin-treated OM (with a pore) and performed unconstrained MD simulations in which four additional colistin A molecules were added above the OM surface. As expected, the pore on the OM was persistent over the entire 100 ns simulation period. Importantly, we found that a newly added colistin A molecule entered the pore in the OM spontaneously (Figure S6a). By contrast, in the same timescale with the untreated bacterial OM, the colistin A molecules only bound to the OM surface and none of the colistin A molecules inserted into the OM (Figure S6b). These results revealed that polymyxin-induced pores in the OM not only increased the permeability of water and ions, but also promoted the penetration of other polymyxin molecules, supporting the 'self-promoted uptake' theory of polymyxin activity proposed in the literature.[44–46]

Discussion

To the best of our knowledge, the present study is the first to employ steered MD simulations and umbrella sampling to reveal, at the all-atomic scale, the unique thermodynamics governing the penetration of polymyxins into the OM of Gram-negative *A. baumannii*. Due to the limited ability of conformational sampling, classical MD simulations cannot track the penetration process of polymyxins into the bacterial OM.[5,6] Enhanced sampling techniques, including umbrella sampling MD simulations and coarse-grained MD simulations, are essential to achieve the penetration of polymyxins within the timescale of simulations.[42] Notably, it is not feasible to investigate the atomic interaction of polymyxins with bacterial membranes using the coarse-grained method, because multiple atoms are considered as one bead in coarse-grained MD.[42] By contrast, all-atom MD simulations[21,23,30] combined with umbrella sampling techniques allow characterization of the interaction of polymyxins with the membrane with an atomic resolution.

The penetration process of polymyxins into the bacterial OM can be divided into three major stages according to the free energy profiles (Figure 3a). First, polymyxin molecules bind to the headgroups of the OM lipids via electrostatic interaction between the cationic Dab residues of polymyxins and the phosphate groups of lipid A (Figure 2c and d). Therefore, it is a common strategy for Gram-negative bacteria to develop polymyxin resistance via modifying the lipid A phosphate groups with moieties (e.g. 4-amino-4-deoxy-L-arabinose and phosphoethanolamine), diminishing the initial interactions with polymyxins.[47,48] Secondly, polymyxin molecules pass across the headgroup region of the OM, during which the free energy increases slowly to approximately 18 kcal/mol for colistin A and approximately 30 kcal/mol for polymyxin B_1. Thirdly, polymyxin molecules traverse the hydrocarbon region of the outer leaflet of the OM, during which the free energy sharply increases to approximately 68 kcal/mol for both polymyxin B_1 and colistin A. During penetration, the polymyxin molecules adopted a folded conformation (Figure 3b), disrupted the cross-linking interactions between adjacent lipid A molecules (Figure 3c) and increased the order of the hydrophobic region of the OM (Figure 3d). These thermodynamic changes represent the entropic penalties of both the polymyxin molecules and the fatty acyl tails
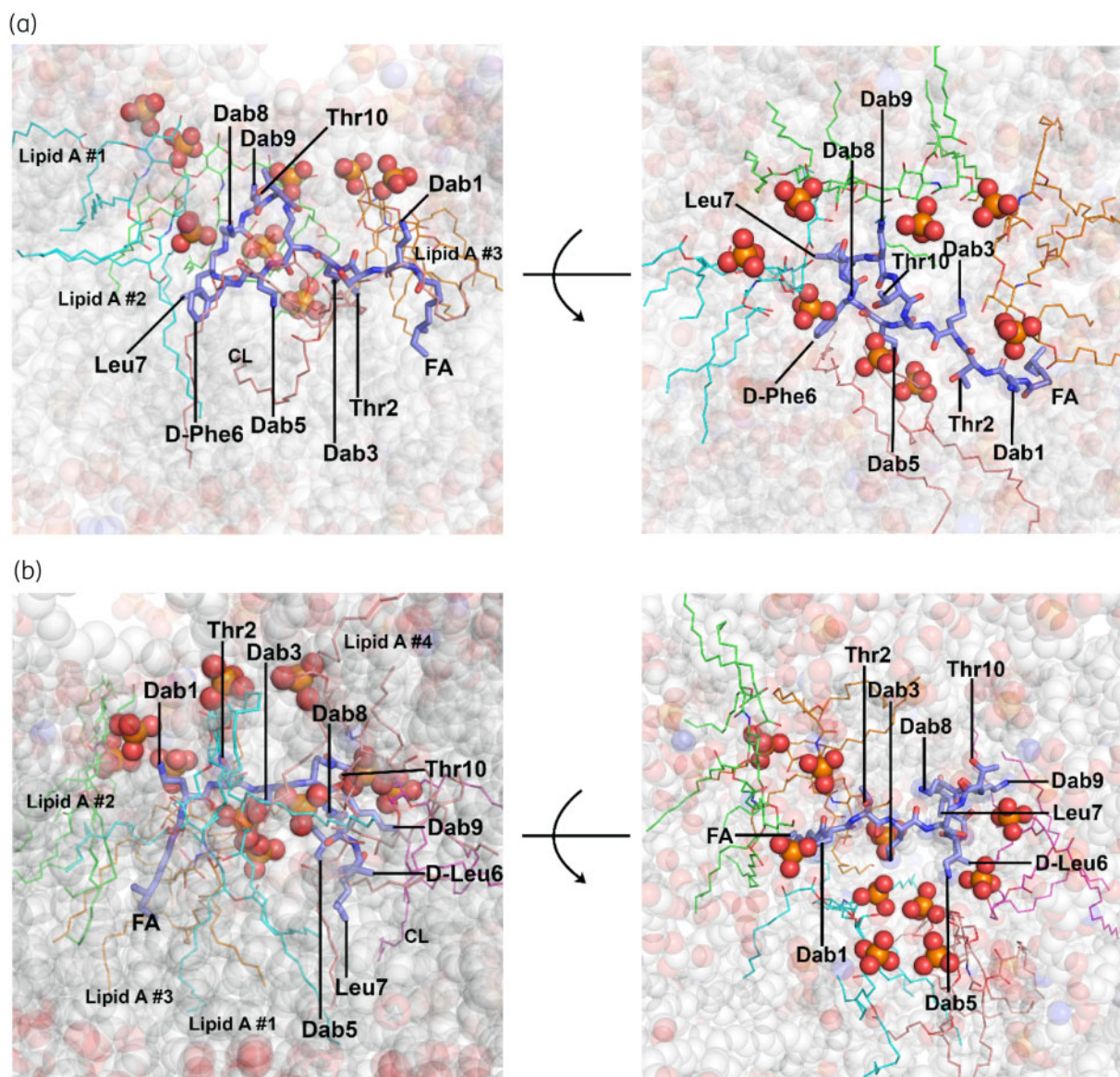
(a)

(b)

Figure 4. Interactions of (a) polymyxin B₁ and (b) colistin A with the OM. Polymyxin molecules are shown as blue stick models. The lipid A and phospholipid molecules interacting with polymyxins are shown as coloured line models, while their phosphate groups are presented as sphere models. The OM is shown as transparent sphere models. This figure appears in colour in the online version of *JAC* and in black and white in the print version of *JAC*.

of lipid A and OM phospholipids and the enthalpic penalty of the headgroups of lipid A and OM phospholipids, which together constitute the free energy barrier of polymyxin penetration into the bacterial OM.[20,42]

Jefferies et al.[42] reported that the free energy for polymyxin penetration into the OM centre was only approximately 10 kcal/mol, lower than the free energy barrier of approximately 68 kcal/mol calculated in the present study. The discrepancy in the free energy barrier likely results from at least two major factors. First, in the previous simulation the polymyxin B₁ molecule did not completely penetrate into the hydrophobic centre of the OM, but primarily stayed in the headgroup region of the OM.[42] However, our results revealed that the free energy barrier for traversing the

polar headgroup region is less than a half of the total free energy barrier (Figure 3a). Secondly, the hydrocarbon tails of lipid A were simplified as two or three beads in the coarse-grained models employed in the previous study,[42] which substantially decreased the thickness and complexity of the OM hydrophobic layer, thus reducing the free energy barrier of polymyxin penetration significantly. In reality, a large number of polymyxin molecules can simultaneously bind to the bacterial OM and disorganize the OM structure cooperatively,[13] which promotes the penetration of polymyxins into the bacterial OM.

With this unique folded conformation (Figure 4), the amphipathic polymyxin molecule specifically interacts with the negatively charged headgroups of lipid A and non-specifically interacts
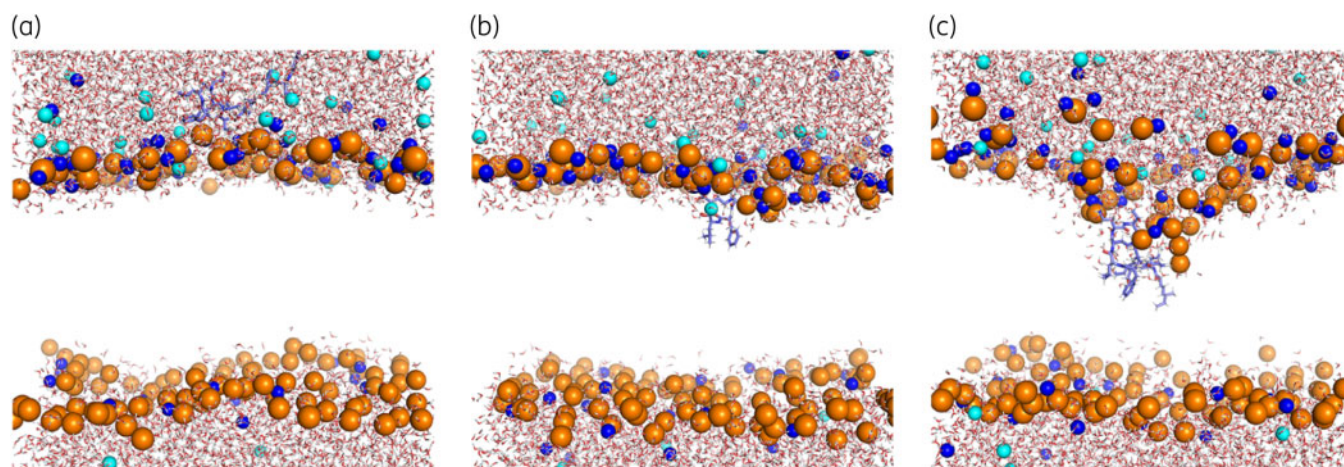
Figure 5. Pore formation in the OM during the penetration of polymyxin B_1. Water molecules are shown as sticks with red oxygen and white hydrogen atoms, polymyxin B_1 is shown as blue sticks and Ca^{2+} and Cl^- are represented by blue and cyan spheres, respectively. The hydrocarbon tails of the membrane lipids are not shown for clarity. Phosphate atoms are shown as orange spheres to represent the positions of the lipid headgroups. This figure appears in colour in the online version of *JAC* and in black and white in the print version of *JAC*.

with the hydrophobic core of lipid A and the OM phospholipids.[41] Previous NMR studies also discovered this folded conformation of polymyxins in the presence of a single lipid A molecule,[14,16] indicating that the folded conformation of polymyxins is a key intermediate state in the penetration into the bacterial OM. However, we should note that the measured distance between the fatty acyl group and Leu7 in the folded conformation of polymyxin B_1 was approximately 1.9 nm in our MD simulations (Figure 3b) and approximately 1.3 nm in a previous NMR study.[49] In the NMR experiments only one lipid A molecule was employed to characterize the interaction mode with polymyxins; therefore, all polar and hydrophobic segments of polymyxin were restrained in the space of a single lipid A molecule. In contrast, in our OM-based all-atom simulations the Dab residues and hydrophobic segments of the polymyxin molecule were able to interact with 3–4 lipid A and phospholipid molecules (Figure 4 and Figure S4). These findings highlight the importance of using lipidomics-informed OM systems in examining the interaction with polymyxins to develop a novel membrane-based structure–activity relationship model of polymyxins.

A recent simulation study examined the permeabilizing effect of polymyxin B;[50] unfortunately, a coarse-grained, symmetric Re-LPS [KDO2-lipid A, consisting of lipid A and 2–3 molecules of 3-deoxy-D-manno-2-octulosonic acid (KDO)] bilayer was used to mimic the bacterial OM,[50] which ignores the heterogeneity of the asymmetric bacterial OM. In contrast, we constructed the *A. baumannii* OM model based on the quantitative lipidomics data.[22] Furthermore, the complete penetration of the polymyxin molecule into the hydrophobic centre of the OM was not examined in previous simulation studies;[5,6,50] therefore, the folded conformation of polymyxins was not observed in those studies, which significantly limits the understanding of the atomic interaction of polymyxins with the bacterial OM. Interestingly, our results revealed that formed pores in the OM promoted the penetration of other polymyxin molecules (Figure S6), supporting a recent experimental study that showed membrane deformation caused by a polymyxin molecule cooperatively enhances the subsequent interactions of other molecules with the bacterial OM.[51] Collectively, our results provide strong support for the 'self-promoted uptake' mechanism of polymyxins in Gram-negative bacteria.[4,8]

To the best of our knowledge, this is the first all-atom study to uncover the thermodynamics of the penetration of the polymyxin molecule into the Gram-negative bacterial OM. Unlike previous studies based on model membranes, the present study employed quantitative membrane lipidomics results to develop an *A. baumannii* OM model for MD simulations. Excitingly, our all-atom simulation results have been utilized to develop a novel membrane-based structure–activity relationship model for polymyxins, which may facilitate the discovery of new-generation polymyxins to combat life-threatening Gram-negative 'superbugs'.

Transparency declarations

None to declare.

Disclaimer

The content is solely the responsibility of the authors and does not necessarily represent the official views of the National Institute of Allergy and Infectious Diseases or the National Institutes of Health.

Supplementary data

Supplementary data, including methods of lipidomics analysis, Figures S1 to S6 and Tables S1 and S2, are available at *JAC* Online.

References

1 WHO. Antimicrobial Resistance Global Report on Surveillance: 2014 Summary. https://www.who.int/drugresistance/documents/surveillancereport/en/.

2 WHO. Global Priority List of Antibiotic-Resistant Bacteria to Guide Research, Discover, and Development of New Antibiotics. https://www.who.int/medicines/publications/global-priority-list-antibiotic-resistant-bacteria/en/.

3 Nation RL, Li J, Cars O *et al.* Framework for optimisation of the clinical use of colistin and polymyxin B: the Prato polymyxin consensus. *Lancet Infect Dis* 2015; **15**: 225–34.

4 Zhang L, Dhillon P, Yan H *et al.* Interactions of bacterial cationic peptide antibiotics with outer and cytoplasmic membranes of *Pseudomonas aeruginosa. Antimicrob Agents Chemother* 2000; **44**: 3317–21.

5 Berglund NA, Piggot TJ, Jefferies D *et al.* Interaction of the antimicrobial peptide polymyxin B1 with both membranes of *E. coli*: a molecular dynamics study. *PLoS Comput Biol* 2015; **11**: e1004180.

6 Santos DES, Pol-Fachin L, Lins RD *et al.* Polymyxin binding to the bacterial outer membrane reveals cation displacement and increasing membrane curvature in susceptible but not in resistant lipopolysaccharide chemotypes. *J Chem Inf Model* 2017; **57**: 2181–93.

7 Domingues MM, Inácio RG, Raimundo JM *et al.* Biophysical characterization of polymyxin b interaction with LPS aggregates and membrane model systems. *Biopolymers* 2012; **98**: 338–44.

8 Hancock RE. Peptide antibiotics. *Lancet* 1997; **349**: 418–22.

9 Piers KL, Brown MH, Hancock RE. Recombinant DNA procedures for producing small antimicrobial cationic peptides in bacteria. *Gene* 1993; **134**: 7–13.

10 Jenssen H, Hamill P, Hancock RE. Peptide antimicrobial agents. *Clin Microbiol Rev* 2006; **19**: 491–511.

11 Vineeth Kumar TV, Sanil G. A review of the mechanism of action of amphibian antimicrobial peptides focusing on peptide-membrane interaction and membrane curvature. *Curr Protein Pept Sci* 2017; **18**: 1263–72.

12 Bennett WF, Hong CK, Wang Y *et al.* Antimicrobial peptide simulations and the influence of force field on the free energy for pore formation in lipid bilayers. *J Chem Theory Comput* 2016; **12**: 4524–33.

13 Velkov T, Thompson PE, Nation RL *et al.* Structure–activity relationships of polymyxin antibiotics. *J Med Chem* 2010; **53**: 1898–916.

14 Velkov T, Roberts KD, Nation RL *et al.* Teaching 'old' polymyxins new tricks: new-generation lipopeptides targeting gram-negative 'superbugs'. *ACS Chem Biol* 2014; **9**: 1172–7.

15 Moore RA, Bates NC, Hancock R. Interaction of polycationic antibiotics with *Pseudomonas aeruginosa* lipopolysaccharide and lipid A studied by using dansyl-polymyxin. *Antimicrob Agents Chemother* 1986; **29**: 496–500.

16 Mares J, Kumaran S, Gobbo M *et al.* Interactions of lipopolysaccharide and polymyxin studied by NMR spectroscopy. *J Biol Chem* 2009; **284**: 11498–506.

17 McInerney MP, Roberts KD, Thompson PE *et al.* Quantitation of polymyxin-lipopolysaccharide interactions using an image-based fluorescent probe. *J Pharm Sci* 2016; **105**: 1006–10.

18 Han ML, Velkov T, Zhu Y *et al.* Polymyxin-induced lipid A deacylation in *Pseudomonas aeruginosa* perturbs polymyxin penetration and confers high-level resistance. *ACS Chem Biol* 2018; **13**: 121–30.

19 Dupuy FG, Pagano I, Andenoro K *et al.* Selective interaction of colistin with lipid model membranes. *Biophys J* 2018; **114**: 919–28.

20 Lin D, Grossfield A. Thermodynamics of antimicrobial lipopeptide binding to membranes: origins of affinity and selectivity. *Biophys J* 2014; **107**: 1862–72.

21 Huang K, Garcia AE. Free energy of translocating an arginine-rich cell-penetrating peptide across a lipid bilayer suggests pore formation. *Biophys J* 2013; **104**: 412–20.

22 Zhu Y, Lu J, Han ML *et al.* Polymyxins bind to the cell surface of unculturable *Acinetobacter baumannii* and cause unique dependent resistance. *Adv Sci* 2020; doi:10.1002/advs.202000704.

23 Khondker A, Dhaliwal AK, Saem S *et al.* Membrane charge and lipid packing determine polymyxin-induced membrane damage. *Commun Biol* 2019; **2**: 67.

24 Jo S, Kim T, Iyer VG *et al.* CHARMM-GUI: a web-based graphical user interface for CHARMM. *J Comput Chem* 2008; **29**: 1859–65.

25 Zoete V, Cuendet MA, Grosdidier A *et al.* SwissParam: a fast force field generation tool for small organic molecules. *J Comput Chem* 2011; **32**: 2359–68.

26 Van Der Spoel D, Lindahl E, Hess B *et al.* GROMACS: fast, flexible, and free. *J Comput Chem* 2005; **26**: 1701–18.

27 Lin D, Grossfield A. Thermodynamics of micelle formation and membrane fusion modulate antimicrobial lipopeptide activity. *Biophys J* 2015; **109**: 750–9.

28 Deshayes S, Morris M, Divita G *et al.* Cell-penetrating peptides: tools for intracellular delivery of therapeutics. *Cell Mol Life Sci* 2005; **62**: 1839–49.

29 Babakhani A, Gorfe AA, Kim JE *et al.* Thermodynamics of peptide insertion and aggregation in a lipid bilayer. *J Phys Chem B* 2008; **112**: 10528–34.

30 Yesylevskyy S, Marrink SJ, Mark AE. Alternative mechanisms for the interaction of the cell-penetrating peptides penetratin and the TAT peptide with lipid bilayers. *Biophys J* 2009; **97**: 40–9.

31 Gu Y, Shrivastava IH, Amara SG *et al.* Molecular simulations elucidate the substrate translocation pathway in a glutamate transporter. *Proc Natl Acad Sci USA* 2009; **106**: 2589–94.

32 Hub JS, de Groot BL, van der Spoel D. g_wham—a free weighted histogram analysis implementation including robust error and autocorrelation estimates. *J Chem Theory Comput* 2010; **6**: 3713–20.

33 Klauda JB, Venable RM, Freites JA *et al.* Update of the CHARMM all-atom additive force field for lipids: validation on six lipid types. *J Phys Chem B* 2010; **114**: 7830–43.

34 Rice A, Rooney MT, Greenwood AI *et al.* Lipopolysaccharide simulations are sensitive to phosphate charge and ion parameterization. *J Chem Theory Comput* 2020; **16**: 1806–15.

35 Parrinello M, Rahman A. Polymorphic transitions in single crystals: a new molecular dynamics method. *J Appl Phys* 1981; **52**: 7182–90.

36 Nosé S. A molecular dynamics method for simulations in the canonical ensemble. *Mol Phys* 1984; **52**: 255–68.

37 Hoover WG. Canonical dynamics: equilibrium phase-space distributions. *Phys Rev A* 1985; **31**: 1695–7.

38 Darden T, York D, Pedersen L. Particle mesh Ewald: an *N*·log (*N*) method for Ewald sums in large systems. *J Chem Phys* 1993; **98**: 10089.

39 Pink D, Truelstrup Hansen L, Gill TA *et al.* Divalent calcium ions inhibit the penetration of protamine through the polysaccharide brush of the outer membrane of Gram-negative bacteria. *Langmuir* 2003; **19**: 8852–8.

40 Pontes FJ, Rusu VH, Soares TA *et al.* The effect of temperature, cations, and number of acyl chains on the lamellar to non-lamellar

transition in lipid-A membranes: a microscopic view. *J Chem Theory Comput* 2012; **8**: 3830–8.

41 Hancock REW. Cationic peptides: effectors in innate immunity and novel antimicrobials. *Lancet Infect Dis* 2001; **1**: 156–64.

42 Jefferies D, Hsu PC, Khalid S. Through the lipopolysaccharide glass: a potent antimicrobial peptide induces phase changes in membranes. *Biochemistry* 2017; **56**: 1672–9.

43 Sun D, Forsman J, Lund M *et al.* Effect of arginine-rich cell penetrating peptides on membrane pore formation and life-times: a molecular simulation study. *Phys Chem Phys* 2014; **16**: 20785–95.

44 Hancock RE. Alterations in outer membrane permeability. *Annu Rev Microbiol* 1984; **38**: 237–64.

45 Wiese A, Münstermann M, Gutsmann T *et al.* Molecular mechanisms of polymyxin B-membrane interactions: direct correlation between surface charge density and self-promoted transport. *J Membr Biol* 1998; **162**: 127–38.

46 Clausell A, Garcia-Subirats M, Pujol M *et al.* Gram-negative outer and inner membrane models: insertion of cyclic cationic lipopeptides. *J Phys Chem B* 2007; **111**: 551–63.

47 Baron S, Hadjadj L, Rolain JM *et al.* Molecular mechanisms of polymyxin resistance: knowns and unknowns. *Int J Antimicrob Agents* 2016; **48**: 583–91.

48 Jeannot K, Bolard A, Plesiat P. Resistance to polymyxins in Gram-negative organisms. *Int J Antimicrob Agents* 2017; **49**: 526–35.

49 Velkov T, Gallardo-Godoy A, Swarbrick JD *et al.* Structure, function, and biosynthetic origin of octapeptin antibiotics active against extensively drug-resistant Gram-negative bacteria. *Cell Chem Biol* 2018; **25**: 380–91.

50 Fu L, Wan M, Zhang S *et al.* Polymyxin B loosens lipopolysaccharide bilayer but stiffens phospholipid bilayer. *Biophys J* 2020; **118**: 138–50.

51 Akhoundsadegh N, Belanger CR, Hancock RE. Outer membrane interaction kinetics of new polymyxin B analogs in Gram-negative bacilli. *Antimicrob Agents Chemother* 2019; **63**: e00935–19.